Available online at www.sciencedirect.com
SCIENCE DIRECT
Journal of Power Sources 147 (2005) 136–147
JOURNAL OF POWER SOURCES
www.elsevier.com/locate/jpowsour

Anode-supported intermediate-temperature direct internal reforming solid oxide fuel cell II. Model-based dynamic performance and control

P. Aguiar [a], C.S. Adjiman [a, b], N.P. Brandon [a, *]

[a] *Department of Chemical Engineering and Chemical Technology, Imperial College London, London SW72AZ, UK*
[b] *Centre for Process Systems Engineering, Imperial College London, London SW72AZ, UK*

Received 24 May 2004; received in revised form 11 January 2005; accepted 17 January 2005
Available online 13 March 2005

Abstract

In operation, solid oxide fuel cells (SOFCs) can be subjected to frequent load changes due to variable power demand. Knowledge of their dynamic behaviour is thus important when looking for suitable control strategies. The present work investigates the open and closed-loop transient response of a co-flow planar anode-supported intermediate-temperature direct internal reforming solid oxide fuel cell to load step-changes. A previously developed dynamic SOFC model, which consists of mass and energy balances and an electrochemical model that relates the fuel and air gas compositions and temperature to voltage, current density, and other relevant fuel cell variables, is used. A master controller that imposes a current density disturbance representing a change in power demand and sets the fuel and air flow rates proportional to that current (keeping the fuel utilisation and air ratio constant) and a typical feedback PID temperature controller that, given the outlet fuel temperature, responds by changing the air ratio around the default set by the master controller, have been implemented. Two distinct control approaches are considered. In the first case, the controller responds to a fixed temperature set-point, while in the second one the set-point is an adjustable parameter that depends on the magnitude of the load change introduced. Open-loop dynamic simulations show that, after a positive/negative load step-change, the overall SOFC temperature increases/decreases and the intermediate period between the disturbance imposed and the new steady-state is characterised by an undershoot/overshoot of the cell potential. Closed-loop simulations when load step-changes from 0.5 to 0.3, 0.4, 0.6, and 0.7 A cm^{-2} are imposed show that the proposed fixed set-point PID controller can successfully take the outlet fuel temperature to the desired set-point. However, it is also shown that for load changes of higher magnitude, an adjustable set-point control strategy is more effective in avoiding oscillatory control action, which can often lead to operation failure, as well as in preventing potentially damaging temperature gradients that can cause excessive stresses within the SOFC components and lead to cell breakdown.

Keywords: Anode-supported; Intermediate-temperature; DIR; SOFC; Dynamic simulation; Control strategy

1. Introduction

Solid oxide fuel cells (SOFCs) are energy conversion devices that produce electricity and heat directly from a gaseous or gasified fuel by electrochemical combination of that fuel with an oxidant. A SOFC consists of an interconnect structure and a three-layer region (often referred to as the PEN—positive-electrode/electrolyte/negative-electrode) composed of two ceramic electrodes, anode and cathode, separated by a dense ceramic electrolyte. SOFCs operate at high temperatures and atmospheric or elevated pressures, and can use hydrogen, carbon monoxide, and hydrocarbons as fuel, and air (or oxygen) as oxidant. In the cell, the oxygen ions formed at the cathode migrate through the ion-conducting electrolyte to the anode/electrolyte interface where they react with the hydrogen and carbon monoxide contained in (and/or produced by) the fuel, producing water and carbon dioxide while releasing electrons that flow via an external circuit to the cathode/electrolyte interface [1].

* Corresponding author. Tel.: +44 20 7594 5704; fax: +44 20 7594 5604.
E-mail address: n.brandon@imperial.ac.uk (N.P. Brandon).

0378-7753/$ – see front matter © 2005 Elsevier B.V. All rights reserved.
doi:10.1016/j.jpowsour.2005.01.017

Nomenclature

F	Faraday's constant (C mol^{-1})
F_{air}	molar flow rate of the air stream (mol s^{-1})
F_{fuel}	molar flow rate of the fuel stream (mol s^{-1})
$\bar{j}$	average current density (A m^{-2})
L	system length (m)
L_{cell}	cell length (m)
LHV_i^0	lower heating value of component i (kJ mol^{-1})
P_{SOFC}	power density (W m^{-2})
T	temperature (K)
U	potential (V)
U_{fuel}	fuel utilisation factor
w_{cell}	cell width (m)
W	system width (m)
x	axial coordinate (m)
y_i	molar fraction of component i
y_i^0	molar fraction of component i at inlet

Greek letters

α	coefficient of thermal expansion (K^{-1})
ε	sustainable stress-induced strain
η_{SOFC}	fuel cell efficiency
λ_{air}	air ratio

Superscripts

0	feed conditions (fuel and air channel inlet)

Subscripts

i	component, $i \in \{CH_4, H_2, CO, O_2\}$
max	maximum
PEN	PEN structure

While conventional high-temperature SOFCs generally operate between 1073 and 1273 K, a number of research groups are presently focusing on intermediate-temperature solid oxide fuel cells (IT-SOFCs). These typically operate between 823 and 1073 K, allowing for a wider range of materials and more cost-effective SOFC fabrication, particularly in relation to the interconnections and balance of plant (BoP). High-temperature SOFCs are generally all ceramic while IT-SOFCs are metal–ceramic and use stainless steel interconnects instead of more expensive high-chrome alloys or oxides. A typical SOFC electrolyte is yttria stabilised zirconia (YSZ), an oxide ion conductor at elevated temperatures. The anode is usually a nickel/zirconia cermet, which provides high electrochemical performance, good chemical stability, and low cost, and the cathode a perovskite material, such as strontium doped lanthanum manganite, often mixed with YSZ in the form of a composite [2,3]. Two main SOFC designs are the electrolyte-supported and electrode-supported SOFC. In the former design, the electrolyte is the thickest component and works as the support structure. Electrolyte-supported cells are only suitable for high-temperature operation where the, often large, ohmic losses can be reduced. Electrode-supported SOFCs have been developed in an attempt to minimise such ohmic losses under lower temperature operation, as in the case of IT-SOFCs. In these cells, one of the two electrodes is the thickest component and support structure, while the electrolyte is required to have high ionic conductivity and/or small thickness. However, it is usually observed that, despite a low ohmic contribution, the area specific resistance of IT-SOFCs may be larger than high-temperature SOFCs. This is due to activation and perhaps concentration overpotentials, which can often outweigh the ohmic contribution. Thus, many of the recent efforts in fuel cell technology development have been devoted to reducing the thickness of critical cell components while improving their structures, with the aim of obtaining a higher and more stable performance with a lower cost [4–6].

Most fuel cells need to convert a hydrocarbon primary fuel into a hydrogen-rich gas required for the electrochemical reaction on the anode side. One option is to process the fuel indirectly in an external catalytic steam reformer or partial oxidation reactor [7]. In the most common case of a reformer, heat needs to be available to drive the endothermic steam reforming reaction. One method of achieving this is to feed the exhaust cell gases into a burner, where the excess fuel is combusted, and the heat generated used to preheat the steam and the fuel and to provide the heat needed in the reformer. However, a more elegant and efficient method of providing heat for the reforming reaction in SOFCs is to carry out the reforming, partially or totally, within the cell stack [8,9]. Internal reforming SOFCs (IR-SOFCs) can eliminate the requirement for a separate fuel reformer and significantly reduce the requirement for cell cooling, usually achieved by flowing excess air through the cathode [10,11]. One approach to IR is direct internal reforming (DIR), where the methane is fed directly into the cell and the reforming takes place directly on the anode [8]. A problem, mostly related to high-temperature SOFCs, is the strong cooling effect caused by the highly endothermic reforming reaction that can generate large temperature gradients across the cell and limit the amount of IR allowed in practice. It has been shown that in high-temperature IR-SOFCs, all the methane is usually completely reformed within a small distance from the anode entrance [12–15]. IT-SOFCs offer significant advantages in terms of internally reforming methane, as the lower temperature naturally reduces the reforming reaction rate [16].

1.1. Complete fuel cell system

For operation, a SOFC must be embedded within a SOFC system incorporating a balance of plant to supply air and clean fuel, convert the direct current (dc) to alternate current (ac), and remove or process the depleted reactants, products, and heat [17–19]. A complete SOFC system is generally composed of five main sub-systems: fuel processing, fuel cell stack, power conditioning, heat recovery and/or further power generation using integrated gas and steam turbines, and plant control. Fig. 1 presents a schematic of such sub-systems. For

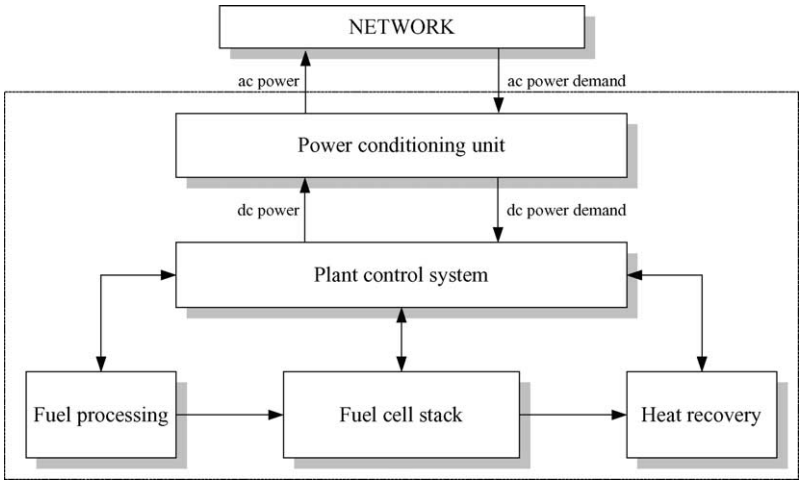

Fig. 1. Schematic of a complete fuel cell system.

a SOFC system, the starting point is the fuel processing: natural gas is first partially or totally externally steam reformed (pre-reformer) before being fed to the SOFC stack, producing hydrogen and carbon monoxide, both of which can be used by the stack as fuel; any natural gas remaining can be reformed internally in the stack, providing useful cooling. The electrochemical power generation takes place when dc electricity is produced within the fuel cells, normally combined in a varying number of cells or stacks that can match a particular power requirement. The power-conditioning unit converts the electric power from direct current into regulated direct current or alternate network current for consumer use. The heat recovery refers to the recovery of residual heat in the exhaust gas that can be used to heat water for local space heating, thus giving a higher overall system efficiency. The control sub-system guarantees that both the BoP and the SOFC stack respond both rapidly and safely to any variation. As expected, all the different elements that compose the SOFC system need to interact closely, i.e., the power conditioning feeds a load demand to which the plant control system needs to react.

1.2. Thermal stresses

Thin film materials, such as the ceramic components of a SOFC, are subjected to stresses that can arise from manufacturing (residual stresses), differences between thermal expansion coefficients, temperature gradients along the cell, oxygen activity gradients, and/or external mechanical loading. In general, a mixture of all these sources of stress is likely to be present and their magnitude depends on the properties of the materials, operating conditions, and design. The strength of a given brittle material is not normally a characteristic of the material itself, but a strong function of the processing conditions, which are being continuously improved; systematic changes in a few processing parameters can lead to residual stress changes of several hundred MPa in metallic and oxide thin films [20].

The high operating temperature of SOFCs implies that the structural stability and reliability of the PEN structure needs to be guaranteed over a wide temperature range. The electrode and electrolyte materials can possess significantly different thermo-mechanical properties, resulting in large thermal stresses during thermal excursions, and failure due to fracture or buckling represents a serious reliability concern [21]. Thus, during the normal operation of a SOFC, the suppression of temperature gradients or transients that can cause excessive stresses within the SOFC components and lead to cell breakdown, is crucial. Therefore, the development of an appropriate control strategy is essential.

As mentioned previously one of the main components of the anode/electrolyte/cathode structure is YSZ and, thus, as a first approximation, mechanical properties of the PEN structure can be taken to be those of a single YSZ layer. Assuming a simple planar structure, the maximum allowable local thermal gradients along the cell can be estimated by

$$\varepsilon_{\max} = \alpha \left.\frac{\mathrm{d}T_{\mathrm{PEN}}}{\mathrm{d}x}\right|_{\max} w_{\mathrm{cell}}, \tag{1}$$

where ε is the sustainable stress-induced strain, α the coefficient of thermal expansion, $\mathrm{d}T_{\mathrm{PEN}}/\mathrm{d}x$ the axial PEN structure temperature gradient, and w_{cell} the cell width. For a square cell, the maximum allowable temperature change $\Delta T_{\max}$ along the cell can then be given by

$$\varepsilon_{\max} = \alpha \frac{\Delta T_{\max}}{L_{\mathrm{cell}}} w_{\mathrm{cell}} = \alpha \Delta T_{\max}, \tag{2}$$

where L_{cell} is the cell length. Therefore, for a coefficient of thermal expansion of $10^{-5}\,\mathrm{K}^{-1}$ [21] and a maximum safe stress-induced strain of 0.1%, the maximum allowable local temperature gradient is $10\,\mathrm{K\,cm}^{-1}$ and the maximum allowable total temperature difference along a 10 cm cell is 100 K. Note that the developed model assumes a total fuel cell length of 40 cm, comprising four individual cells in series, each of 10 cm × 10 cm. Thus, from the results above and the knowledge acquired previously on the SOFC system under study

[16], the total temperature increase along the cell should not represent an operational problem, but special attention should be paid to the local temperature gradients. Thermal stresses resulting from differential thermal expansion or contraction are not considered here.

1.3. Need for dynamic modelling

One of the characteristics of fuel cell systems is that their efficiency is nearly unaffected by size. This means that small, relatively high efficiency power plants can be developed, avoiding the high capital costs normally associated with large plants. Fuel cells are thus suited to distributed generation (DG), which is characterised by small, modular power systems that are sited at or close to the power demand source. DG can be an economic and beneficial addition to commercial buildings, industrial facilities, or any customer dependent on reliable energy. However, while it is known that the operation of a SOFC system is normally subjected to frequent load changes due to variable power demand, its response and, in particular, its interaction with the distributed energy network, is not yet well known. Dynamic modelling is therefore essential for fuel cell systems design, as it allows the prediction of the cell response under transient conditions, and contributes to the definition of appropriate control strategies, not only necessary when load changes occur, but also during start-up or shutdown.

A dynamic model of a planar anode-supported intermediate-temperature direct internal reforming SOFC system is under development. The project is divided in two main tasks: dynamic modelling of a SOFC stack alone, presented here, and subsequent dynamic modelling of the whole SOFC system, to be presented in the near future. These models can be used to study the dynamics of the SOFC stack and remaining BoP, producing an improved understanding of their interaction, to investigate possible control strategies, and to study design changes.

The aim of this publication is to present the dynamic behaviour of a solid oxide fuel cell and to discuss appropriate control strategies for this type of system. For that purpose, the response of a planar anode-supported IT DIR-SOFC to load step-changes is analysed under both open-loop and closed-loop conditions. The next section briefly describes the dynamic SOFC model developed and the control strategy adopted.

2. SOFC dynamic simulation and control strategy

2.1. SOFC stack model

There have been several publications focusing on modelling the performance of high-temperature SOFCs. Such models can be for different geometries, PEN structures, and flow configurations; can range from one to three-dimensional; and can consider or not IR or various other phenomena [1,12,22–27]. Even though most of the work reported describes SOFC steady-state performance, dynamic issues have also been addressed by some authors. Ota et al. [28] and Hall and Colclaser [29] analysed the open-loop transient response of a high temperature tubular SOFC to small load step-changes, while Achenbach [30,31] presented a similar study for a planar SOFC.

In a previous publication, Part I [16], the authors presented a dynamic anode-supported intermediate-temperature direct internal reforming planar co-flow one-dimensional SOFC model, which is used in the present work. To produce a useful voltage, a SOFC consists of several repeating electrochemical cells in a module, connected both in series and/or in parallel and assembled to compose a stack. However, SOFC models are usually developed for the smallest unit cell or module, then used to compute the operating conditions of the whole stack. In the case reported here, the repeating single-cell is considered to be in the centre of a large stack, such that no edge effects are present, and to be formed when two interconnect plates are placed above and below the cell PEN structure. A schematic side view of a co-flow SOFC stack, where the unit cell being modelled is indicated, is illustrated in Fig. 2. For the model, the SOFC was considered to be composed of fuel and air channels, PEN structure, and interconnect. The model consists of mass balances around the fuel and air channels, energy balances around the fuel and air channels, PEN, and interconnect, and an electrochemical model that relates the fuel and air gas compositions and the various cell temperatures to voltage, current density, and other cell variables. The chemical species considered are CH_4, H_2O, CO, H_2, and CO_2 for the fuel stream and O_2 and N_2 for the air stream. It is assumed that only H_2 is electrochemically oxidised, all the CO is converted through the water-gas shift reaction, assumed at equilibrium, and any CH_4 in the fuel can only be reformed to H_2, CO, and CO_2 but not electrochemically oxidised. The electrochemical model accounts for ohmic losses across the PEN structure and for anode and cathode concentration and activation overpotentials.

For the model solution, in addition to all geometry and property data and inlet temperatures and compositions, it is

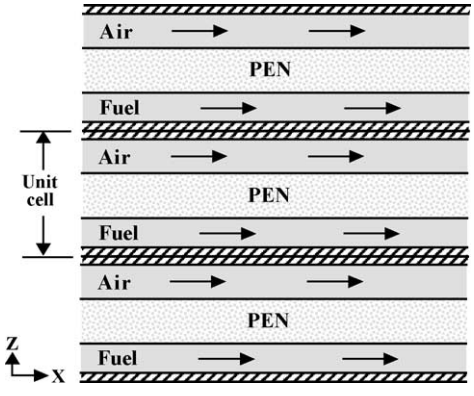

Fig. 2. Schematic side view of a co-flow planar SOFC stack.

Table 1
Mathematical definition of fuel utilisation, air ratio, and fuel efficiency

Fuel utilisation	$U_{\text{fuel}} = \dfrac{\bar{j}LW}{(8Fy^0_{\text{CH}_4} + 2Fy^0_{\text{H}_2} + 2Fy^0_{\text{CO}})F^0_{\text{fuel}}}$	(3)
Air ratio	$\lambda_{\text{air}} = \dfrac{y^0_{\text{O}_2} F^0_{\text{air}}}{jLW/4F}$	(4)
Power density	$P_{\text{SOFC}} = jU$	(5)
Fuel efficiency	$\eta_{\text{SOFC}} = \dfrac{P_{\text{SOFC}}LW}{(y^0_{\text{CH}_4}\,\text{LHV}^0_{\text{CH}_4} + y^0_{\text{H}_2}\,\text{LHV}^0_{\text{H}_2} + y^0_{\text{CO}}\,\text{LHV}^0_{\text{CO}})F^0_{\text{fuel}}}$	(6)

necessary to specify the average current density, fuel utilisation, and air ratio (from which the molar flux of fuel and air are determined). Fuel utilisation is defined as the fraction of the inlet fuel that is used to produce electricity, and the air ratio as the excess air, in relation to that stoichiometrically needed, that is supplied for cooling. The fuel efficiency is defined as the fraction of the chemical energy in the inlet fuel that is converted to electric power. Table 1 presents the mathematical definition of these performance factors. The resulting system of partial differential and algebraic equations is solved using *gPROMS ModelBuilder* 2.2.5 [32], with the finite difference integration method. All remaining details of the model developed can be found in Ref. [16].

2.2. Possible control strategy

An effective control strategy aims to avoid any possible failure conditions. These can include limitations in temperature variation, to avoid the thermal stresses described above, practical limits on fuel and air flow rates, or a maximum allowable variation of the electrochemical variables. Common requirements for the operation of a SOFC include: controlling the average stack temperature and guaranteeing that the outlet gas temperature is as constant as possible (at least across the full to 50% power operating range); maintaining the fuel utilisation constant for all power outputs; and ensuring that the air ratio always exceeds a minimum specified value. However, when the complete SOFC system is considered, many other requirements need to be satisfied. A simple example is the lower limit normally imposed on the steam to carbon ratio at the entrance of the pre-reformer to avoid carbon deposition.

The present publication focuses on the behaviour of the SOFC stack alone and on the discussion of a possible control strategy that satisfies some of the above requirements. Stack temperature control is normally provided by varying the air ratio, i.e., the supply of air for cooling. Although in practice the stack temperature could be taken as the average reading of several thermocouples placed at different locations, here only the outlet fuel gas temperature is controlled. Since the inlet fuel and air temperature are set a priori (boundary conditions for the model), this approximation assumes that the variation of the average cell temperature is limited to a certain extent although not precisely controlled. The maximum temperature gradients achieved along the cell, mentioned in Section 1.2, are monitored even if no control loop is implemented for their control.

Two main control loops have been implemented: a master controller that imposes a current density disturbance (as if a change in power demand occurs) and sets the fuel and air flow rates proportional to that current; and a typical feedback proportional–integral–derivative (PID) temperature controller that, given the outlet fuel gas temperature, responds by changing the air flow around the default air flow set by the master controller. The master controller maintains constant fuel utilisation and air ratio according to the definitions given in Table 1. In feedback control the objective is to reduce the error signal between a pre-defined set-point and the measured value of the controlled variable [33]. Under PID control, the controller output depends on the error signal (proportional action), on its integral over time (integral action), and on its rate of change (derivative action). Such controllers have three tuning parameters that can be adjusted to make the changes in the controller output as sensitive as desired to deviations between set-point and controlled variable. For the PID temperature controller above, the controlled variable is the outlet fuel gas temperature, the manipulated variable is the air flow rate, and the set-point defined remains constant. Note that the remainder of this paper distinguishes between open-loop and closed-loop system response; closed-loop implies that both the above control loops are active, whereas open-loop suggests that only the master controller is in operation, i.e., there is no temperature control. Bounds are set on the operation of the PID controller, where the air ratio cannot be assigned a value below 2 (minimum stoichiometrically needed air plus a safety margin) and above 14 (compressor maximum allowed air flow rate). Previous publications [28–30] on the open-loop load change behaviour of SOFCs have assumed a constant fuel flow rate throughout any load change.

In practice, one other control loop, not implemented here, would monitor the variation of cell voltage because of changes in current density and guarantee that such voltage does not fall below a certain specified value. A fuel cell is normally designed to operate within a voltage range of 0.6–0.7 V, although higher or lower voltage values are allowed. This voltage range is a compromise between low capital cost, efficiency, stable operation, and anode oxidation prevention at low voltage. Table 2 summarises the operation limits discussed.

Table 2
Summary of limits on cell operation

Desired outlet fuel temperature (K)	1123
Allowed air ratio range	2–14
Desired operating voltage range (V)	0.6–0.7
Minimum allowed cell voltage value (V)	0.55
Maximum allowed local PEN temperature gradient (K cm^{-1})	10

3. Simulation results and discussion

The model described above is able to predict the various cell temperatures (fuel and air channels, PEN structure, and interconnect), the gas composition (fuel and air channels), and all the electrochemical-related variables (open-circuit voltage, activation, ohmic, and concentration overpotential losses, terminal potential, current density) along the cell length as well as their variation with time.

3.1. Initial steady-state conditions

To study the effect of load changes on SOFC performance, an initial steady-state needs to be defined. For this steady-state, the composition of the inlet fuel results from a fuel mixture with a steam to carbon ratio equal to 2 after 10% pre-reforming, where the shift reaction is at equilibrium. The operating pressure is 1 bar and the temperature of the fuel and air inlet streams is 1023 K. The current density considered is 0.5 A cm^{-2}, with a fuel utilisation of 75%, and an air ratio value of 8.93 (value chosen to achieve an outlet fuel temperature of 1123 K). The remaining model input geometry and property data can be found in Ref. [16].

The steady-state performance of such a SOFC, as well as the impact of changes in inlet temperatures, fuel utilisation, average current density, and flow configuration, have been previously illustrated [16]. For the above operating conditions, the SOFC operates at an output voltage of 0.664 V, a power density of 0.332 W cm^{-2}, and a fuel efficiency of 46.8%. Fig. 3 illustrates some characteristic profiles for the steady-state defined above: fuel channel component mole fraction profiles, and fuel and air channels, PEN structure, and interconnect temperature profiles along the cell length.

Fig. 3a demonstrates the impact of the simultaneous occurrence of the DIR, water gas-shift, and hydrogen oxidation reactions. At the entrance of the fuel cell, and due to the high methane content, the reforming reaction is much faster and the methane is consumed rapidly, producing hydrogen and carbon monoxide. Once most of the methane is consumed, the hydrogen oxidation reaction becomes dominant and the consumption of hydrogen and production of steam can be clearly seen. Fig. 3b shows that the cell temperature increases along the direction of fuel and air flow, with the maximum temperature occurring at the outlet. Although the reforming reaction is known to be strongly endothermic, the total heat consumed by the DIR reaction represents only 45% of the total heat produced in the cell, and only a slight local cooling effect caused by this reaction is observed at the cell entrance: the fuel channel temperature decreases by 53 K in relation to its inlet value (the equivalent temperature decrease in the PEN structure is around 17 K). However, it should be pointed out that, while this is true for the operating conditions and kinetic data used in the present model, temperature gradients due to DIR should always be carefully monitored. If these prove to be detrimental for the operation of a particular SOFC, the degree of methane pre-reforming (here set to 10%) and the anode material (more precisely, its activity to steam reforming) are some of the factors that may be manipulated. For the remaining of this paper and as the PEN temperatures gradients due to DIR never exceed the maximum defined in Table 2, only the temperature gradients due to the heat accumulation along the gas flow direction are monitored (Figs. 5 and 11). Finally, all the

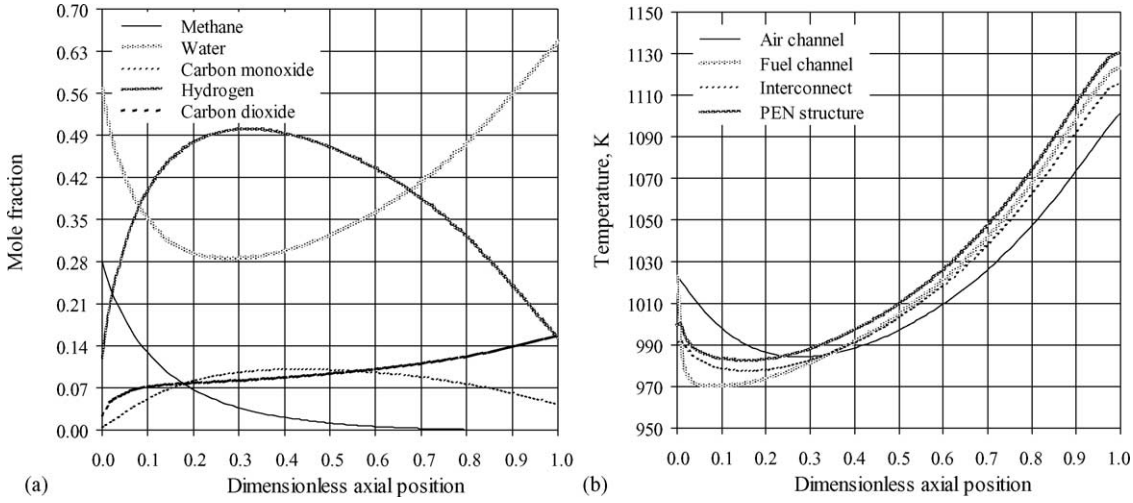

Fig. 3. Fuel channel component mole fractions (a) and fuel and air channels, PEN structure, and interconnect temperature (b) profiles along the cell length for the initial steady-state conditions.

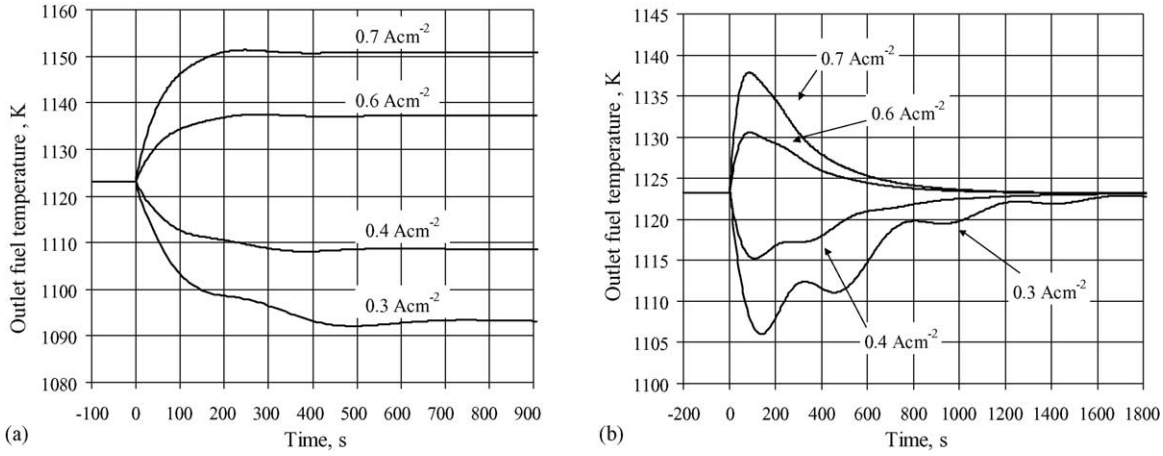

Fig. 4. Open-loop (a) and closed-loop (b) transient response of the outlet fuel temperature for 0.5 (initial steady-state conditions) to 0.3, 0.4, 0.6, and 0.7 A cm^{-2} load step-changes.

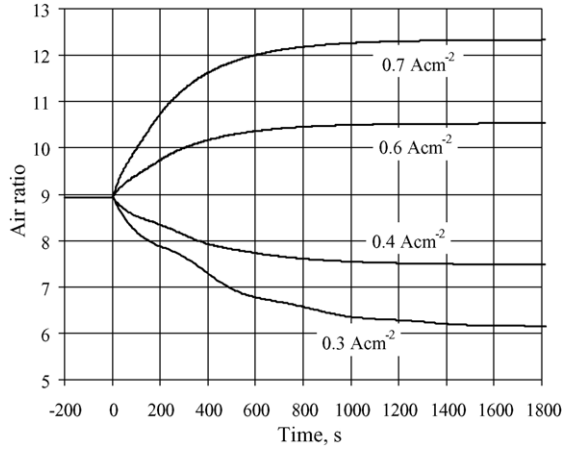

Fig. 5. Closed-loop air ratio transient response for 0.5 (initial steady-state conditions) to 0.3, 0.4, 0.6, and 0.7 A cm^{-2} load step-changes.

conditions in Table 2 are satisfied for these initial steady-state conditions: the overall fuel stream temperature increase along the cell is 100 K and, although the maximum temperature difference in the PEN structure is around 148 K, the maximum local PEN temperature gradient does not exceed 8.3 K cm^{-1}.

3.2. SOFC stack response to load step-changes: fixed PID controller set-point

Figs. 4–8 illustrate the transient stack behaviour, under open-loop and closed-loop conditions, when load step-changes from 0.5 to 0.3 and 0.4 A cm^{-2} (negative load changes) and to 0.6 and 0.7 A cm^{-2} (positive load changes) are imposed. These four disturbances were chosen to illustrate the stack behaviour when both positive and negative symmetric load changes occur. Table 3 presents the corresponding new steady-state values of some relevant variables (outlet fuel temperature, cell potential, fuel efficiency, and air ratio) for both the open-loop and closed-loop cases. Note that the PID controller implemented has not been comprehensively tuned; the parameters used (controller gain = 0.5 (reverse action), reset time = 100, derivative time = 100, and derivative time limit = 100) were found to provide fast system response, although oscillations for negative load changes are

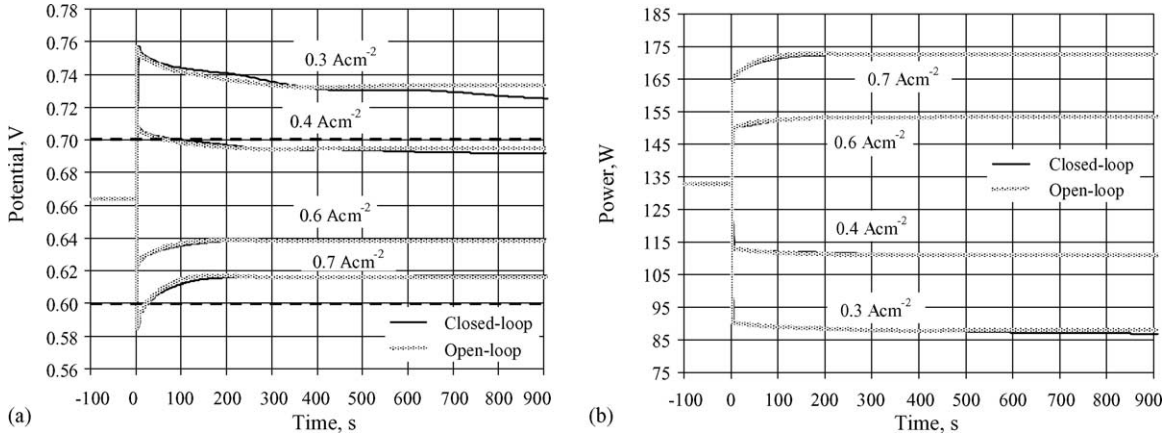

Fig. 6. Open-loop and closed-loop transient response of the cell potential (a) and cell power output (b) for 0.5 (initial steady-state conditions) to 0.3, 0.4, 0.6, and 0.7 A cm^{-2} load step-changes. The dashed lines in (a) show the desirable operating voltage range.

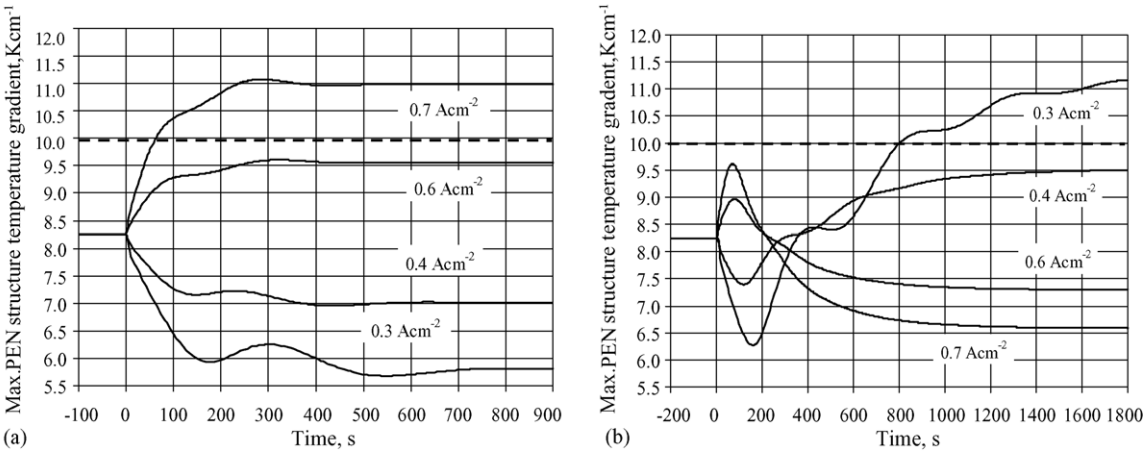

Fig. 7. Open-loop (a) and closed-loop (b) transient response of the maximum PEN structure temperature gradient for 0.5 (initial steady-state conditions) to 0.3, 0.4, 0.6, and 0.7 A cm^{-2} load step-changes. The dashed lines show the maximum allowed local PEN temperature gradient.

Table 3
Initial and new steady-state values for 0.5 to 0.3, 0.4, 0.6, and 0.7 A cm^{-2} load changes

	Final current density (A cm^{-2})				
	0.5	0.3	0.4	0.6	0.7
	Initial	Open-loop case			
Outlet fuel temperature (K)	1123	1093.2	1108.6	1137.2	1150.8
Cell potential (V)	0.664	0.733	0.695	0.638	0.616
Fuel efficiency (%)	46.8	51.7	49.0	45.0	43.5
		Closed-loop case			
Cell potential (V)		0.722	0.691	0.640	0.617
Fuel efficiency (%)		50.9	48.7	45.1	43.5
Air ratio		6.10	7.47	10.5	12.3

still observed. The desired outlet fuel temperature and, thus, the PID controller set-point is, according to Table 2, 1123 K.

Fig. 4 presents the outlet fuel temperature transient behaviour after the introduction of the above load disturbances.

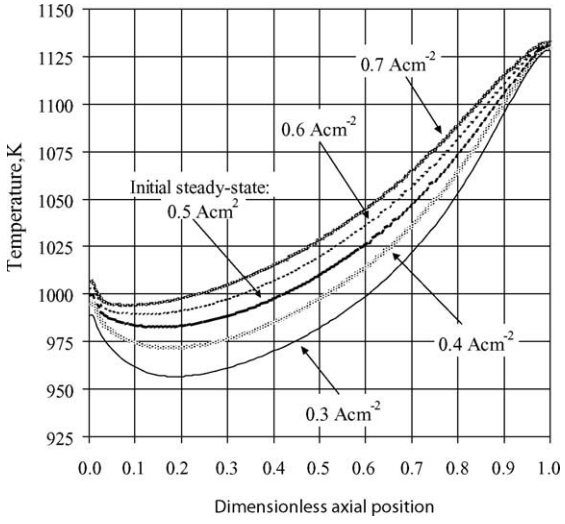

Fig. 8. Closed-loop PEN structure temperature profile at the new steady-state for 0.5 (initial steady-state conditions) to 0.3, 0.4, 0.6, and 0.7 A cm^{-2} load step-changes.

As can be seen, for the open-loop case (no temperature control), the temperature increases for positive load changes and decreases for negative ones, while for the closed-loop case, the PID controller successfully and progressively brings the temperature back to the specified 1123 K set-point. The controller takes around 1000 s to stabilise the outlet fuel temperature (the fuel residence time varies from 0.71 to 0.30 s).

Fig. 5 presents the air ratio transient variation that results from the PID controller action. As mentioned before, the fuel and air flow rates are set by the master controller to follow any variation in current density, keeping the fuel utilisation and air ratio constant. This occurs for both open-loop and closed-loop cases. The air flow rate (air ratio) is varied by the PID controller around the value set by the master controller to maintain the outlet fuel temperature at the desired set-point (closed-loop case only). As seen from Fig. 5, the air ratio increases/decreases for positive/negative load changes to avoid the fuel temperature increase/decrease that would otherwise be observed (Fig. 4a). The controlled variable for the 0.5 to 0.3 A cm^{-2} load change case (Fig. 4b) presents more oscillations than for the other cases. In addition, it is important to point out that, for higher negative load step-changes (for instance, 0.5 to 0.2 or 0.1 A cm^{-2}), the control strategy proposed is no longer able to take the system temperature to

the specified set-point, and irreversible and progressively increasing oscillations are observed instead. This can be explained by two contributing factors. The first one is related to the limitations associated with the use of a PID controller: a PID controller can only guarantee a good performance if any introduced disturbance does not imply a significant change in the operating point, i.e., if the new steady-state is not considerably different from the initial one. The second factor is related to the fact that, as the magnitude of the negative load change imposed increases, the controller reduces the air ratio to an extent where the cell operation becomes very sensitive to any further changes, resulting in the oscillations described. An alternative control approach, found more appropriate for significant load changes, is discussed in the next section. Although for high positive load changes such oscillations are not observed, it is believed that such an alternative approach is also beneficial in these cases, as it allows for the reduction of the otherwise very high cell temperature, while avoiding excessively high air flow rates.

Fig. 6 presents the transient response of both the cell potential and the cell power output for the same conditions as above. It can be seen that the intermediate period between the imposed disturbance and the new steady-state is characterised by an undershoot (for positive load changes) or an overshoot (for negative load changes) of the cell potential. As is well known, a SOFC is less/more efficient for higher/lower current density values, causing a larger/smaller production of waste heat with a consequent temperature increase/decrease. In addition, it is clear that the changes taking effect have different characteristic response times: changes in gas flow rates and power output are much faster than changes in temperature. These factors explain the undershoot/overshoot phenomena observed in Fig. 6: as immediately after the current density step-change, the cell temperature is still low/high (and related to the initial current density value), all the sources of voltage loss are higher/lower at that point. Therefore, during that intermediate period, the cell voltage is lower/higher than the new steady-state value. It is also important to stress that, though for the closed-loop case the outlet fuel temperature remains approximately constant (Fig. 4b), the average cell temperature does increase/decrease for positive/negative load changes. Therefore, both cases undergo the same undershoot/overshoot effects. Any differences in the cell potential transient behaviour (undershoot/overshoot and new steady-state values) between the open-loop and closed-loop cases are due to those differences in temperature. Only the 0.5 to 0.3 A cm^{-2} load change case shows a final cell voltage outside the desirable operating voltage range presented in Table 2, although the undershoot/overshoot does go below/above that range for a few seconds for the 0.4 and 0.7 A cm^{-2} case loads. Since there is no information available at present that implies any potentially damaging effects caused by these short undershoot phenomena, the SOFC dynamic response is found acceptable. In addition, in relation to the 0.5 to 0.3 A cm^{-2} load change case, although it is important to understand the system behaviour under these conditions, it is not expected, for economical reasons, that the SOFC in question would operate under these or lower current densities for a long period. Fig. 6b illustrates that the power output responds proportionally to the load disturbance introduced. As can be seen, the voltage undershoot/overshoot phenomena are reflected on the power output curve (Fig. 6b), which does not respond immediately to the load change imposed, but increases/decreases progressively to the new steady-state value. Overall, the open-loop simulation results presented show the same general response reported by Achenbach [30] for a planar SOFC and by Hall and Colclaser [29] for a tubular SOFC.

Fig. 7 presents the transient response of the maximum PEN structure temperature gradient for the disturbances imposed. It is interesting to note that, while for the open-loop case, higher PEN temperature gradients (where the maximum allowed local PEN temperature gradient of 10 K cm^{-1} is exceed) are associated with the positive load change cases (higher final current density values), the opposite is true when temperature control is in operation. For the cases where an increase in load occurs, this trend seems logical, as the action of the controller causes a reduction in the fuel outlet temperature, smoothing the cell temperature profiles. However, as discussed before, for the cases where a decrease in current density occurs, the controller acts by decreasing the air ratio, increasing the fuel outlet temperature and making the temperature profiles steeper. The fact that the SOFC in question performs DIR, contributes to an even less uniform temperature distribution within the cell (although, as mentioned before, temperature gradients caused by DIR do not exceed 10 K cm^{-1}). Fig. 8 illustrates the axial PEN structure temperature profiles for the new steady-states, providing a clearer picture of the PEN structure temperature gradients just mentioned.

3.3. SOFC stack response to load step-changes: adjustable PID controller set-point

The above discussion demonstrates that, if thermal stresses within a SOFC under normal operation are an issue of concern, a more flexible control strategy is required to avoid undesirable temperature gradients induced by a controller action that tries to meet a fixed temperature set-point. In other words, the control action should respond according to the disturbance introduced. This section illustrates the case where the set-point is not fixed for any of the possible disturbances imposed to the system but is instead an adjustable value that depends on the magnitude of each disturbance. The PID temperature controller is, otherwise, similar to the one implemented in Section 3.2. Four more simulation cases are presented: load step-changes from 0.5 to 0.3 and 0.2 A cm^{-2} under open-loop and closed-loop conditions. For the closed-loop cases, the set-point is decreased by 25 and 50 K for the 0.5 to 0.3 and 0.5 to 0.2 A cm^{-2} load change cases, respectively. Although the decrease in set-point has

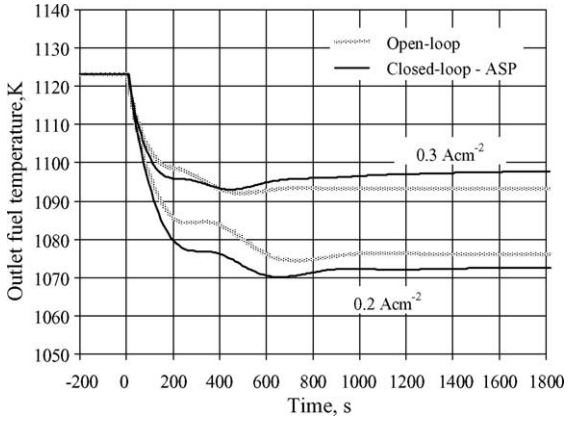

Fig. 9. Open-loop and closed-loop transient response of the outlet fuel temperature for 0.5 to 0.2 and 0.3 A cm^{-2} load step-changes for an adjustable controller set-point.

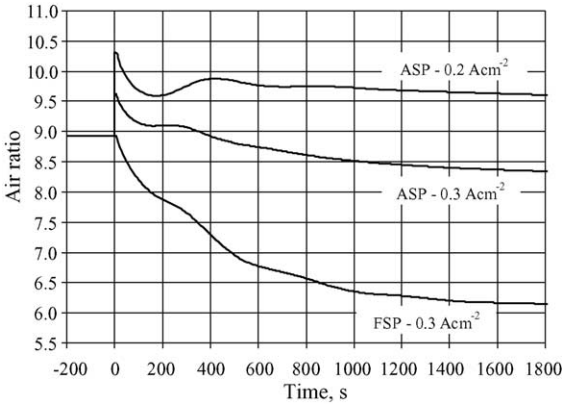

Fig. 10. Closed-loop air ratio transient response for 0.5 to 0.2 and 0.3 A cm^{-2} load step-changes for both fixed and adjustable controller set-point.

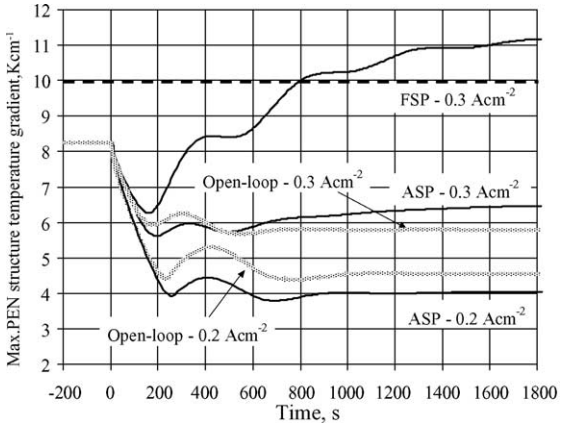

Fig. 11. Open-loop and closed-loop transient response of the maximum PEN structure temperature gradient for 0.5–0.2 and 0.3 A cm^{-2} load step-changes for both fixed and adjustable controller set-point. The dashed lines show the maximum allowed local PEN temperature gradient.

been, at this stage, chosen by the authors, this could be a value predicted by a model-based technique. Only negative load changes are used to illustrate this new control approach, although a similar approach could also be applied for high positive load changes (to avoid excessive air flow rates). The case where a load disturbance from 0.5 to 0.3 A cm^{-2} is introduced is repeated here to compare the system performance under both control strategies. The case where a load disturbance from 0.5 to 0.2 A cm^{-2} is introduced was chosen to demonstrate that the successful performance of a particular cell under a given load disturbance depends largely on the control strategy adopted. Figs. 9–11 illustrate the transient stack behaviour, under open-loop (OL) and closed-loop (CL) conditions for the disturbances just described. There are two closed-loop sub-cases: fixed set-point (FSP) and adjustable set-point (ASP). As for the controller parameters, the values presented in Section 3.1 are also used here. Table 4 presents the corresponding new steady-state values.

Fig. 9 presents the outlet fuel temperature transient behaviour after the introduction of the above load disturbances. As can be seen, for the closed-loop ASP case, the PID controller successfully and progressively takes the temperature to the specified set-point of 1098 and 1073 K (adjustable set-point) for a load change from 0.5 to 0.3 and 0.2 A cm^{-2}, respectively. Note that, by applying such a temperature decrease, both the open-loop and closed-loop cases have similar final temperatures. From Fig. 9, it can be seen that the outlet fuel temperature takes around 1000 s to stabilise.

Fig. 10 presents the closed-loop air ratio transient response for 0.5 to 0.2 and 0.3 A cm^{-2} load step-changes for both fixed and adjustable controller set-point cases. No FSP case is shown for the case of a step load change of 0.5 to 0.2 A cm^{-2} as no stable solution exists for this case. As can be seen from Fig. 10, the final air ratio for the 0.5 to 0.3 A cm^{-2} load change case with an ASP is higher than the one with a FSP

Table 4
New steady-state values for 0.5 to 0.2 and 0.3 A cm^{-2} load changes

	Final current density (A cm^{-2})				
	0.2		0.3		
	OL	CL-ASP	OL	CL-FSP	CL-ASP
Outlet fuel temperature (K)	1076.2	1073.1	1093.2	1123.2	1098.1
Cell potential (V)	0.783	0.784	0.733	0.722	0.731
Fuel efficiency (%)	55.2	55.3	51.7	50.9	51.6
Air ratio	8.93	9.48	8.93	6.10	8.29

(in accordance with the set-point decrease) and for the 0.5 to 0.2 A cm^{-2} load change case a stable performance is now possible. The small changes in air ratio implemented by the controller lead to the small temperature differences observed in Fig. 9 between the open and closed-loop cases. It can be observed that the air ratio takes longer to stabilise than the outlet fuel temperature.

The transient response of the cell potential is similar to the results in Fig. 6a. The final potential value for the 0.5 to 0.3 A cm^{-2} load change case with the FSP approach is lower that the one for the ASP approach (see Table 4), as the average cell temperature for the former case is lower (even though the outlet cell temperature is higher).

Fig. 11 presents the transient response of the maximum PEN structure temperature gradients. While in Section 3.2 it was concluded that a FSP control approach leads to high temperature gradients for negative load changes, it can be seen that the new ASP approach is efficient in decreasing those gradients.

4. Concluding remarks

The dynamic response of a planar intermediate-temperature anode-supported direct internal reforming SOFC to several current density step-changes has been presented. Two main control loops have been implemented. The first loop is composed of a master controller that imposes a load change and sets the fuel and air flow rates proportional to that new current, keeping the fuel utilisation and air ratio constant. The second one is a feedback PID temperature controller that, given the outlet fuel temperature, responds by changing the air flow (air ratio) around the default value set by the master controller. Simulation results for both a fixed and an adjustable set-point control strategy for the outlet fuel temperature have been presented. It has been shown that, for load changes of moderate magnitude, the PID temperature controller can successfully take the outlet fuel temperature to the desired set-point. However, for load changes of higher magnitude, an adjustable set-point strategy is more appropriate in avoiding oscillatory control action as well as in preventing potentially damaging temperature stresses. Independently of the control strategy, the controller takes around 1000 s to stabilise the outlet fuel temperature. Although a more complex control approach is required for the complete SOFC system, the control strategy proposed so far is considered appropriate.

Finally, it is worth noting that many other factors need to be carefully addressed when controlling SOFC systems for which a model of the full SOFC system is required. For instance, if the voltage variations observed above prove to be of any risk (operation safety or cell durability), there are still two degrees of freedom that can be manipulated. One is the fuel utilisation, that can have a significant impact on the cell terminal voltage, and the other is the fuel composition, which depends greatly on the performance of the fuel pre-reformer. There are also some issues related to the control strategy itself. While a PID feedback approach has been adopted here, a number of other more refined control strategies could easily be applied to the fuel cell field. In the case of model predictive control, for instance, the control algorithm would predict a priori the outlet fuel temperature expected after the measured load change and take the necessary advanced control action to avoid any temperature increase or decrease. Nevertheless, the results presented above seem to imply that, although the operation of a solid oxide fuel cell is complex, both the cell temperature variation and the air ratio required for controlling it can be easily predicted after a current density change (within a certain range). Therefore, in addition to a typical PID control, use could be made of a simple entry driven table that would automatically decide on the new air ratio value (the PID controller would always be in place for safety reasons). An equivalent approach could be applied together with the adjustable set-point control approach, where such a table would provide the appropriate set-point values. This simplified approach would be helpful in the more realistic case of frequent load changes for which a faster system response is needed.

References

[1] J.R. Ferguson, J.M. Fiard, R. Herbin, Three-dimensional numerical simulation for various geometries of solid oxide fuel cells, J. Power Sources 58 (1996) 109–122.
[2] O. Yamamoto, Solid oxide fuel cells: fundamental aspects and prospects, Electrochim. Acta 45 (2000) 2423–2435.
[3] S.P.S. Badwal, K. Foger, Solid oxide electrolyte fuel cell review, Ceram. Int. 22 (1996) 257–265.
[4] J.P.P. Huijsmans, Ceramics in solid oxide fuel cells, Curr. Opin. Solid State Mater. Sci. 5 (2001) 317–323.
[5] S.H. Chan, K.A. Khor, Z.T. Xia, A complete polarization model of a solid oxide fuel cell and its sensitivity to the change of cell component thickness, J. Power Sources 93 (2001) 130–140.
[6] A.V. Virkar, J. Chen, C.W. Tanner, J. Kim, The role of electrode microstructure on activation and concentration polarizations in solid oxide fuel cells, Solid State Ionics 131 (2000) 189–198.
[7] A.L. Dicks, Advances in catalysts for internal reforming in high temperature fuel cells, J. Power Sources 71 (1998) 111–122.
[8] S.H. Clarke, A.L. Dicks, K. Pointon, T.A. Smith, A. Swann, Catalytic aspects of the steam reforming of hydrocarbons in internal reforming fuel cells, Catal. Today 38 (1997) 411–423.
[9] J. Rostrup-Nielsen, L.J. Christiansen, Internal steam reforming in fuel cells and alkali poisoning, Appl. Catal. A: Gen. 126 (1995) 381–390.
[10] N. Nakagawa, H. Sagara, K. Kato, Catalytic activity of Ni–YSZ–CeO_2 anode for the steam reforming of methane in a direct internal-reforming solid oxide fuel cell, J. Power Sources 92 (2001) 88–94.
[11] A.L. Lee, R.F. Zabransky, W.J. Huber, Internal reforming development for solid oxide fuel cells, Ind. Eng. Chem. Res. 29 (1990) 766–773.
[12] P. Aguiar, D. Chadwick, L. Kershenbaum, Modelling of an indirect internal reforming solid oxide fuel cell, Chem. Eng. Sci. 57 (2002) 1665–1677.
[13] R. Fellows, A novel configuration for direct internal reforming stacks, J. Power Sources 71 (1998) 281–287.

[14] J. Meusinger, E. Riensche, U. Stimming, Reforming of natural gas in solid oxide fuel cell systems, J. Power Sources 71 (1998) 315–320.
[15] E. Achenbach, E. Riensche, Methane/steam reforming kinetics for solid oxide fuel cells, J. Power Sources 52 (1994) 283–288.
[16] P. Aguiar, C.S. Adjiman, N.P. Brandon, Anode-supported intermediate-temperature direct internal reforming solid oxide fuel cell: model-based steady-state performance, J. Power Sources 138 (2004) 120–136.
[17] K. Joon, Fuel cells—a 21st century power system, J. Power Sources 71 (1998) 12–18.
[18] EG&G Services, Parsons, Inc., Science Applications International Corporation, Fuel Cell Handbook, 5th ed., U.S. Department of Energy, Office of Fossil Energy, National Energy Technology Laboratory, Virginia, 2000.
[19] J. Padullés, G.W. Ault, J.R. McDonald, An integrated SOFC plant dynamic model for power systems simulation, J. Power Sources 86 (2000) 495–500.
[20] V.T. Srikar, K.T. Turner, T.Y.A. Ie, S.M. Spearing, Structural design considerations for micromachined solid-oxide fuel cells, J. Power Sources 125 (2004) 62–69.
[21] A. Atkinson, A. Selçuk, Mechanical behaviour of ceramic oxygen ion-conducting membranes, Solid State Ionics 134 (2000) 59–66.
[22] K.P. Recknagle, R.E. Williford, L.A. Chick, D.R. Rector, M.A. Khaleel, Three-dimensional thermo-fluid electrochemical modeling of planar SOFC stacks, J. Power Sources 113 (2003) 109–114.
[23] S. Nagata, A. Momma, T. Kato, Y. Kasuga, Numerical analysis of output characteristics of tubular SOFC with internal reformer, J. Power Sources 101 (2001) 60–71.
[24] M. Iwata, T. Hikosaka, M. Morita, T. Iwanari, K. Ito, K. Onda, Y. Esaki, Y. Sakaki, S. Nagata, Performance analysis of planar-type unit SOFC considering current and temperature distributions, Solid State Ionics 132 (2000) 297–308.
[25] S.G. Neophytides, The reversed flow operation of a crossflow solid oxide fuel cell monolith, Chem. Eng. Sci. 54 (1999) 4603–4613.
[26] N.F. Bessette II, W.J. Wepfer, J. Winnick, A mathematical model of a solid oxide fuel cell, J. Electrochem. Soc. 142 (1995) 3792–3800.
[27] S. Ahmed, C. McPheeters, R. Kumar, Thermal-hydraulic model of a monolithic solid oxide fuel cell, J. Electrochem. Soc. 138 (1991) 2712–2718.
[28] T. Ota, M. Koyama, C. Wen, K. Yamada, H. Takahashi, Object-based modeling of SOFC system: dynamic behavior of micro-tube SOFC, J. Power Sources 118 (2003) 430–439.
[29] D.J. Hall, R.G. Colclaser, Transient modeling and simulation of a tubular solid oxide fuel cell, IEEE Trans. Energy Conversion 14 (1999) 749–753.
[30] E. Achenbach, Response of a solid oxide fuel cell to load change, J. Power Sources 57 (1995) 105–109.
[31] E. Achenbach, Three-dimensional and time-dependent simulation of a planar solid oxide fuel cell stack, J. Power Sources 49 (1994) 333–348.
[32] Process Systems Enterprise Ltd., gPROMS Introductory User Guide, Process Systems Enterprise Ltd., London, 2002.
[33] D.E. Seborg, T.F. Edgar, D.A. Mellichamp, Process Dynamics and Control, Wiley, 1989.